N. J. M. van Dijk[1]
Department of Mechanical Engineering,
Eindhoven University of Technology,
P.O. Box 513,
5600 MB Eindhoven, The Netherlands
e-mail: n.j.m.v.dijk@tue.nl

E. J. J. Doppenberg
TNO Science and Industry,
P.O. Box 6235,
5600 HE Eindhoven, The Netherlands

R. P. H. Faassen
TMC Mechatronics.
P.O. Box 700,
5600 AS Eindhoven, The Netherlands

N. van de Wouw
Department of Mechanical Engineering,
Eindhoven University of Technology,
P.O. Box 513,
5600 MB Eindhoven, The Netherlands

J. A. J. Oosterling
TNO Science and Industry,
P.O. Box 6235,
5600 HE Eindhoven, The Netherlands

H. Nijmeijer
Department of Mechanical Engineering,
Eindhoven University of Technology,
P.O. Box 513,
5600 MB Eindhoven, The Netherlands

Automatic In-Process Chatter Avoidance in the High-Speed Milling Process

High-speed milling is often used in industry to maximize productivity of the manufacturing of high-technology components, such as aeronautical components, mold, and dies. The occurrence of chatter highly limits the efficiency and accuracy of high-speed milling operations. In this paper, two control strategies are presented that guarantee a chatter-free high-speed milling operation by automatic adaptation of spindle speed and feed. Moreover, the proposed strategies are robust for changing process conditions (e.g., due to heating of the spindle or tool wear). An important part of the control strategy is the detection of chatter. A novel chatter detection algorithm is presented that automatically detects chatter in an online fashion and in a premature phase such that no visible marks on the workpiece are present. Experiments on a state-of-the-art high-speed milling machine underline the effectiveness of the proposed detection and control strategies.
[DOI: 10.1115/1.4000821]

1 Introduction

One of the main goals in high-speed machining is to maximize the material removal rate while maintaining a high quality level of the workpiece. The material removal rate is often limited by the occurrence of chatter. This instability phenomenon results in an inferior workpiece surface quality due to heavy vibrations of the tool. Furthermore, the tool and machine wear out rapidly and a high level of noise is produced. Different types of chatter exist, see, e.g., Ref. [1]. However, the focus in this work lies on the prevention of full grown chatter of the prevalent type, i.e., regenerative chatter.

The combination of the demands for high productivity at a high quality level and the increasing demands for an automated process calls for an automatic chatter detection and control system [2].

This paper presents two chatter control strategies that, by automatic (and online) adaptation of spindle speed and feed, guarantee chatter-free high-speed machining operations while productivity is maintained. The first control strategy follows the methodology as presented in Ref. [3]; i.e., stable machining is guaranteed when a tooth-passing frequency equals the dominant chatter frequency. The novelty of the first control strategy, with respect to the work in Ref. [3], is that the spindle speed is changed in an online fashion when chatter is about to occur. As will be shown by experiments, stable machining is ensured, even for spindle speed over 30,000 rpm.

Setting a spindle speed harmonic equal to the dominant chatter frequency, in general, implies that chatter vibrations will be bounded but not likely to be minimized. Therefore, a second control strategy is presented that automatically lowers the cutter vibrations associated with chatter via real-time adaptation of spindle speed and feed.

Both control strategies require an accurate estimate of the dominant chatter frequency before chatter marks are visible on the workpiece. Current chatter detection methods [4–9] might work well for low spindle speeds but they either utilize too much computational time to be able to detect chatter before it has already developed toward the fully grown stage or are not able to estimate the dominant chatter frequency. A notable exception is the work presented in Ref. [10], where an online chatter detection methodology in the case of turning, is presented. Based on a discrete autoregressive moving average model, chatter modes are estimated from the vibration signal. Since in the case of milling the vibration signal also consists of spindle-speed related frequencies [11], the method presented in Ref. [10] cannot directly be used for the milling process. Hence, the third contribution of the paper is to present a novel chatter detection algorithm, based on a parametric model of the milling process, that detects chatter when it is in a premature stage; i.e., no chatter marks are visible on the workpiece yet, and, moreover, give an accurate estimate of the dominant chatter frequency.

In literature, basically three methods exist to avoid or overcome chatter. The first method is to disturb the regeneration process by

[1]Corresponding author.

Contributed by the Dynamic Systems Division of ASME for publication in the Journal of Dynamic Systems, Measurement, and Control. Manuscript received April 15, 2009; final manuscript received November 23, 2009; published online April 21, 2010. Assoc. Editor: Marcio de Queiroz.

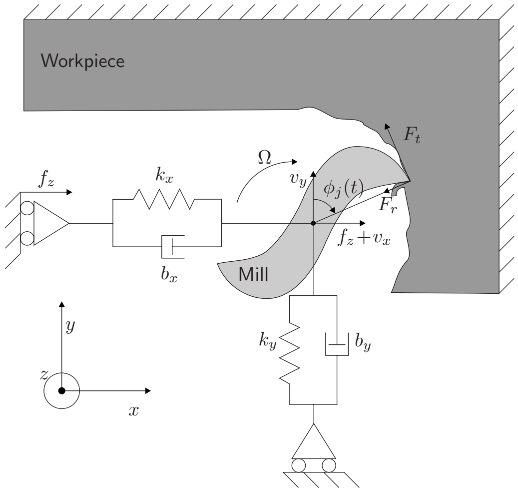

Fig. 1 Schematic representation of the milling process

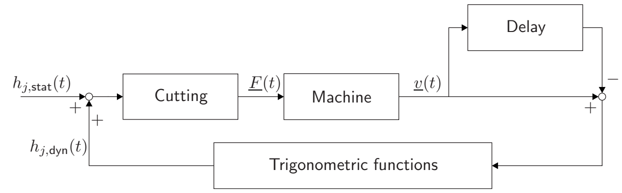

Fig. 2 Block diagram of the milling process

constantly changing the spindle speed [12,13]. This method cannot be used in high-speed milling due to the high spindle speeds. In order to disturb the regenerative effect, the spindle-speed variation should be extremely fast, while the speed of variation is limited by the inertia and actuation power of the spindle. A second method is to passively or actively alter the machine dynamics in order to increase the critical depth of cut. Passive chatter suppression techniques exist in the form of dampers [14] or vibration absorbers [15]. Active dampers for milling are suggested in Ref. [16] for low-speed milling, and also in Ref. [17] an active control strategy is developed for low-speed milling. The third method to avoid chatter is to adjust the process parameters (i.e., spindle speed, chip load, or depth of cut) such that a stable working point is chosen [5]. In the Chatter Recognition and Control (CRAC) system, chatter is detected by examining the audio spectrum of a cut [18]. When chatter is detected, the feed is interrupted and a new spindle speed is set. Then, the feed is resumed. This process is repeated until no chatter occurs. Since chatter is detected using a microphone, it can only be detected when it is already in a highly developed stage and the workpiece is already damaged. Furthermore, stopping and restarting the feed leave marks on the workpiece and increase production time. In Ref. [19], a method is presented where feed is not interrupted. However, the method is only applicable for low spindle speeds due to computational effort of the detection signal, which requires a buffer of sensor data. Moreover, the spindle speed can only be ramped up, which may result in chatter during the spindle-speed transition. In Ref. [20], new spindle speed and feedrate setpoints are based on a heuristic search for stable machining conditions.

Resuming, the main contributions of this paper are, first, a chatter detection strategy for high-speed milling, which is fast enough to detect chatter before it has fully grown, and, second, presenting the design of constructive control strategies, guaranteeing the avoidance of chatter by adapting the spindle speed and feed in an online fashion before chatter marks are visible on the workpiece.

This paper is organized as follows. In Sec. 2, a brief background of the milling process and chatter is presented. In Sec. 3, the detection algorithm is described, including the selection of the sensor system. In Sec. 4, the two chatter control strategies are described. Experimental results using the detection and control strategies are discussed in Sec. 5. Finally, conclusions are drawn in Sec. 6.

2 The Milling Process

In Fig. 1, a schematic representation of the milling process is shown, and a block diagram of the milling model is shown in Fig. 2.

The total chip thickness of tooth j, $h_j(t)$, is the sum of the static and dynamic chip thickness, $h_j(t)=h_{j,\mathrm{stat}}(t)+h_{j,\mathrm{dyn}}(t)$. The static chip thickness $h_{j,\mathrm{stat}}(t)$ is a result of the predefined motion of the tool with respect to the workpiece and is described by $h_{j,\mathrm{stat}}(t)=f_z \sin \phi_j(t)$, with $\phi_j(t)$ the rotation angle of tooth j and f_z the chip load. This chip thickness results, via the cutting process (block Cutting in Fig. 2), in a cutting force $\underline{F}(t)$ that acts on the tool. The forces in tangential and radial directions are described by the following exponential cutting force model:

$$F_{t_j}(t) = (K_t a_p h_j(t)^{x_F} + K_{te} a_p) g_j(\phi_j(t))$$

$$F_{r_j}(t) = (K_r a_p h_j(t)^{x_F} + K_{re} a_p) g_j(\phi_j(t)) \tag{1}$$

where $0 < x_F \leq 1$, $K_t, K_r > 0$, and $K_{te}, K_{re} \geq 0$ are the cutting parameters that depend on the material that is cut, and a_p is the axial depth of cut. The function $g_j(\phi_j(t))$ describes whether a tooth is in or out of cut: $g_j(\phi_j(t))=1$ when $\phi_s \leq \phi_j(t) \leq \phi_e \wedge h_j(t) > 0$ and $g_j(\phi_j(t))=0$ elsewhere. Via trigonometric functions, the cutting force can easily be converted to x (feed) and y (normal) directions. This force interacts with the spindle and tool dynamics (block Machine in Fig. 2), modeled via a linear state-space model,

$$\dot{\underline{z}}(t) = \mathbf{A}\underline{z}(t) + \mathbf{B}\underline{F}(t), \quad \underline{v}(t) = \mathbf{C}\underline{z}(t) \tag{2}$$

where $\underline{z}$ is the state (the order of this model primarily depends on the order of the spindle-tool dynamics model) and $\underline{F}(t)=[F_x(t) \;\; F_y(t)]^T$, where $F_x(t)$ and $F_y(t)$ are the cutting forces in x and y directions, respectively. This results in a dynamic displacement of the tool $\underline{v}(t)$, which is superimposed on the predefined tool motion. The dynamic chip thickness is the result of this displacement $\underline{v}(t)=[v_x(t) \;\; v_y(t)]^T$ and the displacement of the cutter at the previous tooth pass at time $\underline{v}(t-\tau)$, where τ is the delay. This is called the regenerative effect and results in the block Delay in Fig. 2 (see, e.g., Ref. [21]). Via trigonometric relations, the tool motion results in a dynamic chip thickness $h_{j,\mathrm{dyn}}(t)$, which is added to the static chip thickness. Hence, when summing for all Z teeth, the cutting forces in the x- and y-directions can be described by

$$\underline{F}(t) = a_p \sum_{j=0}^{Z-1} g_j(\phi_j(t)) \Bigg((h_{j,\mathrm{stat}}(t) + [\sin \phi_j(t) \quad \cos \phi_j(t)] \times (\underline{v}(t) - \underline{v}(t-\tau)))^{x_F} \mathbf{S}(t) \begin{bmatrix} K_t \\ K_r \end{bmatrix} + \mathbf{S}(t) \begin{bmatrix} K_{te} \\ K_{re} \end{bmatrix} \Bigg) \tag{3}$$

where

$$\mathbf{S}(t) = \begin{bmatrix} -\cos \phi_j(t) & -\sin \phi_j(t) \\ \sin \phi_j(t) & -\cos \phi_j(t) \end{bmatrix}$$

Substitution of Eq. (3) in Eq. (2) yields the delay differential equations describing the milling process:

$$\dot{\underline{z}}(t) = \mathbf{A}\underline{z}(t) + \mathbf{B} a_p \sum_{j=0}^{Z-1} g_j(\phi_j(t)) \Bigg((h_{j,\mathrm{stat}}(t) + [\sin \phi_j(t) \quad \cos \phi_j(t)] \times \mathbf{C}(\underline{z}(t) - \underline{z}(t-\tau)))^{x_F} \mathbf{S}(t) \begin{bmatrix} K_t \\ K_r \end{bmatrix} + \mathbf{S}(t) \begin{bmatrix} K_{te} \\ K_{re} \end{bmatrix} \Bigg)$$

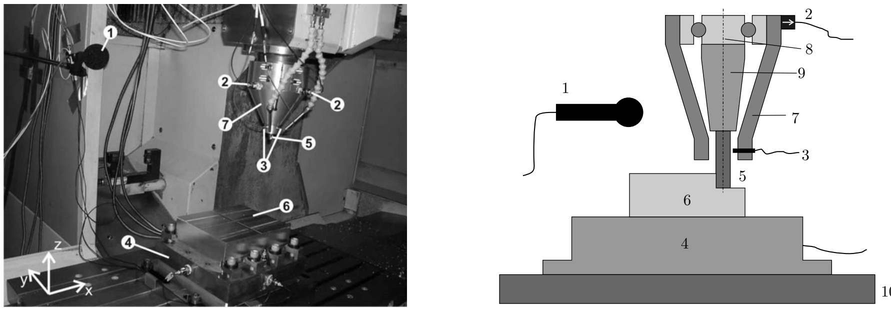

(*a*) Photo (*b*) Schematic representation

Fig. 3 The setup: (1) microphone, (2) accelerometers, (3) eddy current sensors, (4) dynamometer, (5) tool, (6) workpiece, (7) mounting device, (8) spindle, (9) toolholder, and (10) bed

$$\underset{\sim}{v}(t) = \mathbf{C}\underset{\sim}{z}(t) \tag{4}$$

In the milling process, the static chip thickness is periodic. The motion $\underset{\sim}{v}(t)$ of the cutter can therefore be described by a periodic motion $\underset{\sim}{v}_p(t)$, which is, in the case of a concentric tool, periodic with period time $\tau=1/f_t=60/Z\Omega$. Here, f_t denotes the tooth-passing frequency, Z is the number of teeth on the cutter, and Ω is the spindle speed in rpm. A perturbation on that periodic movement is denoted by $\underset{\sim}{v}_u(t)$, i.e., $\underset{\sim}{v}(t)=\underset{\sim}{v}_p(t)+\underset{\sim}{v}_u(t)$. If no chatter occurs, the periodic movement $\underset{\sim}{v}_p(t)$ is an asymptotically stable solution of the set of delay differential equations describing the milling process and the perturbation $\underset{\sim}{v}_u(t)$ tends to zero asymptotically. When the periodic solution loses its stability (e.g., with an increasing axial depth of cut), in most cases a secondary Hopf bifurcation occurs and in other cases a period doubling bifurcation occurs [11]. This means that the original periodic solution $\underset{\sim}{v}_p(t)$ becomes unstable and a new periodic motion with a different frequency f_c is superimposed on the original periodic solution. In the remainder of this paper, we will call f_c the basic chatter frequency. In general, the following frequencies appear in the vibration signals [11]: (multiples of) the tooth-passing excitation frequency, $f_{\mathrm{TPE}}=kf_t$, with $k\in\mathbb{Z}^+$, and the damped natural frequency of the spindle-toolholder-tool (STT) combination, $f_d=f_n\sqrt{1-\zeta^2}$, with f_n the undamped natural frequency of the STT and ζ the dimensionless damping. In an unstable cut, the following frequencies can occur additionally [11]: chatter frequencies due to a secondary Hopf bifurcation:

$$f_H = \pm f_h + kf_t \quad \text{with} \quad k=0, \pm 1, \pm 2, \ldots \tag{5}$$

or chatter frequencies due to a period doubling bifurcation:

$$f_{\mathrm{PD}} = f_{pd} + kf_t = \left(k+\frac{1}{2}\right)f_t \quad \text{with} \quad k=0, \pm 1, \pm 2, \ldots \tag{6}$$

When chatter occurs, the energy of the vibration at the frequencies related to f_c significantly increases. Since the chatter frequencies represent a large set of discrete frequencies, one of these frequencies will generally lie close to a natural frequency of the STT system and will consequently be dominant in the vibration signals. This frequency will be called the dominant chatter frequency f_{chat} in the remainder of this paper. In practice, basically three stages in the development of chatter can be identified. In the first phase, no chatter is occurring. This implies that the frequency spectrum of the vibration signals only consists of spindle-speed related frequencies and no chatter marks are visible on the workpiece. In the second phase, the frequency spectrum of the vibration signals consists of spindle-speed related frequencies and the dominant chatter frequency. However, no chatter marks are visible on the workpiece yet. This phase is called onset of chatter. The third phase is called full grown chatter. The frequency spectrum consists of spindle-speed related frequencies and chatter frequencies f_H or f_{PD}. Moreover, chatter marks are visible on the workpiece. The goal of the detection method is to detect onset of chatter and identify the dominant chatter frequency, needed for control, in real time before chatter marks are left on the workpiece.

3 Chatter Detection

In this section, the real-time chatter detection strategy will be presented. The main objective of the chatter detection is, first, to detect onset of chatter in an early stage of its growth and, second, to identify the dominant chatter frequency. Based on the outcome of the detection method, a control action (in this case adjusting spindle speed and feed) will be effected to ensure that the process remains stable and full grown chatter is avoided. As already mentioned in the Introduction, the detection and control action must be performed in real time due to the rapid growth of chatter for high spindle speeds. Clearly, the choice of an appropriate sensor is essential in a control system. Therefore, we present in Sec. 3.1 an experimental comparative study performed on a Mikron HSM 700 milling machine, using a wide range of sensors to select an appropriate sensor for chatter detection. In Sec. 3.2, the real-time detection strategy will be presented.

3.1 Sensor Choice. A picture of the milling machine is shown in Fig. 3(*a*) and the setup is schematically depicted in Fig. 3(*b*). The following sensors have been used: a microphone, accelerometers at the spindle housing in feed (x) and normal (y) direction, eddy current sensors measuring the displacement of the tool in the x- and y-directions, and a dynamometer for force measurements. The tool used is a 10 mm diameter JH420 cutter with two teeth and the workpiece material is aluminum. Due to lack of space, the results are presented for only one working point. However, comparative results are obtained for different working points. Measurements are performed for a cut where the mill is rotating at 42,000 rpm. The axial depth of cut is 2 mm and the chip load is 0.15 mm/tooth. The radial depth of cut is increased from 4 mm to 6 mm, which results in the occurrence of chatter during the cut. In Fig. 4, a power spectral density plot of the acceleration at the spindle bearing in the y-direction is shown. Due to runout not only the tooth-passing frequencies, denoted by f_{TPE}, can be seen from the measured signals but also the spindle speed itself and its higher harmonics. We will denote the latter frequencies by f_{SP}. This frequency is exactly half the tooth-passing frequency since the tool has two teeth.

As can be seen, due to an eccentricity in the STT combination, the basic chatter frequency $f_c=96$ Hz is also added to or subtracted from all f_{SP} instead of f_{TPE}. For these experiments the demodulation method, see Ref. [8], is used as chatter detection method. The demodulation method will only be used for sensor

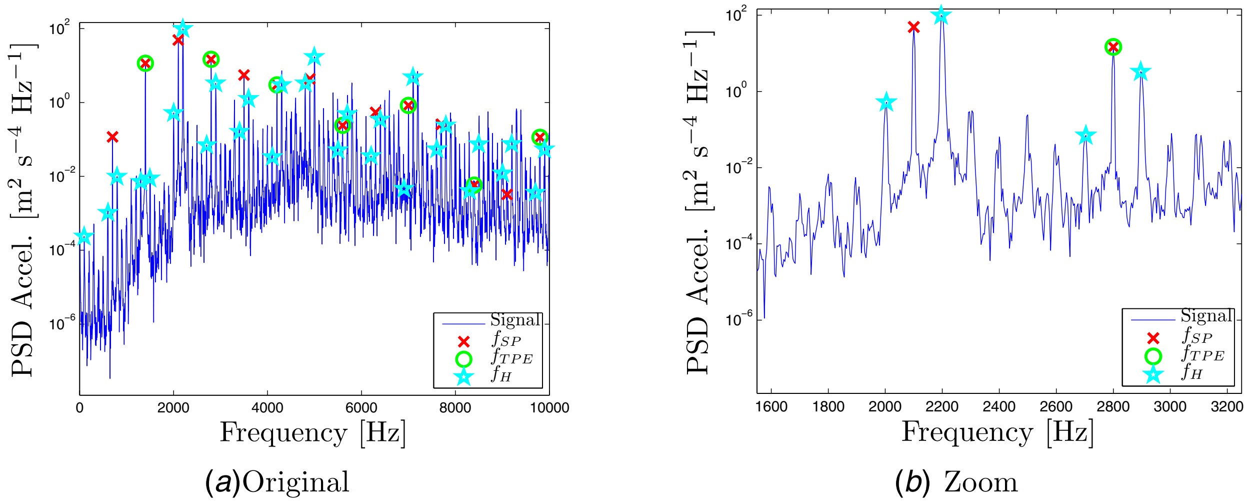

Fig. 4 Power spectral density of the measured acceleration in the *y*-direction in the case of chatter

selection. Although the demodulation method can be used for chatter detection, it cannot be used for chatter control since the dominant chatter frequency cannot be determined. For this method, a choice for the demodulation frequency must be made. Since the dominant chatter frequency lies around the third harmonic of the spindle speed, the chosen frequency at which the demodulation is performed is three times the spindle speed: $f_1 = 3(\Omega/60)$ Hz. In Fig. 5, the detection signal is presented for several sensors. At $t=0$, the tool enters the cut. During the first part of the cut, no chatter occurs, which results in a low value of the detection signal. When chatter begins (around $t=0.6$ s), the amplitude of the chatter frequency rises and, consequently, the value of the detection signal increases rapidly. Just after $t=1$ s, the tool leaves the cut. In all signals presented here, the increase in the detection signal at $t=0.6$ s can be observed. However, the increase is relatively large in the displacement and acceleration signals. Moreover, during the stable part of the cut, these signals show the lowest noise level. When a threshold would be set just above the maximum value of the signals of the first part, chatter is detected 50 ms earlier when acceleration or displacement sensors are used compared with force or sound measurements. This time is significant when realizing that at high spindle speeds chatter typically arises in approximately 100 ms. The increase in the sound signal happens in two parts. This is due to the acoustic environment in the milling cage.

A major drawback of using eddy current sensors is the fact that a special mounting device is necessary and that these sensors are quite expensive. Using force signals for online chatter detection requires the workpiece to be mounted on the dynamometer. This is not desirable for use in an industrial environment. Moreover, the measured force vibration signal in the case of milling consists of spindle-speed related signals and possible chatter frequencies, which may lie close to the eigenfrequency of a dynamometer. Therefore, from a combined detection performance and cost effectiveness point of view, an accelerometer mounted near the lower spindle bearing is preferable.

3.2 Chatter Detection Via Parametric Modeling. Besides the detection of the onset of chatter, also knowledge on the chatter frequency f_{chat} is essential in the desired control strategy (see Sec. 4). This asks for a parametric modeling approach of the milling process, which will be presented Sec. 3.2.1. In Sec. 3.2.2, the estimation of the parameters of the model will be presented. The real-time implementation of the estimation of the parameters is presented in Sec. 3.2.3. Finally, the procedure for detection of the onset of chatter is discussed in Sec. 3.2.4.

3.2.1 Parametric Modeling of the Milling Process. From Sec. 3.1, it is concluded that chatter is detected earlier when using acceleration sensors instead of force or sound sensors. Here, one accelerometer is used for chatter detection. This section presents a model of the milling process, using the measured acceleration $a(t)$, without the necessity constructing a complete cutting process model, as presented in Sec. 2.

As described in Sec. 2, the movement of the cutter $v(t)$ is composed of a periodic part $v_p(t)$ and perturbation part $v_u(t)$. The same decomposition can be used for the acceleration $a(t)$: $a(t) = a_p(t) + a_u(t)$. The digital representation of the milling process can then be written as an output error model [22], which is of the following form:

$$a(kT_s) = G(q)u(kT_s) + H(q)e(kT_s) \tag{7}$$

Herein the sequence $a(kT_s)$, $k=0,1,\ldots$, is the digital representation of the continuous signal $a(t)$ with T_s the sampling interval, $u(kT_s)$input signal, $e(kT_s)$ Gaussian white noise with zero-mean and variance σ^2, and $G(q)$ and $H(q)$ rational minimum phase transfer functions, which are a function of the shift operator q. In the remainder, the sampling interval T_s is omitted for notational convenience, i.e., $a(k) \coloneqq a(kT_s)$. The signal model of the periodic component $a_p(k)$ can now be denoted as $a_p(k) = G(q)u(k)$, and the signal model of the perturbation part $a_u(k)$ can be denoted as $a_u(k) = H(q)e(k)$. A common model structure for Eq. (7) is the Box–Jenkins (BJ) model, see, e.g., Ref. [22]. Its general formulation is as follows:

$$a(k) = \frac{B(q)}{F(q)}u_{\text{ref}}(k) + \frac{C(q)}{D(q)}e(k). \tag{8}$$

Here, $e(k)$ is again Gaussian white noise of zero-mean and variance σ^2 and $u_{\text{ref}}(k)$ is the input, due to the spindle-speed related perturbation, which can be composed by a discrete cosine/sine series, with the spindle speed as the fundamental frequency, given by

$$u_{\text{ref}}(k) = \sum_{l=1}^{L} u^l(k) = \sum_{l=1}^{L} \begin{bmatrix} \cos(l\omega(k)kT_s) \\ \sin(l\omega(k)kT_s) \end{bmatrix} \tag{9}$$

Herein, $\omega(k) = 2\pi\Omega(k)/60$, with $\Omega(k)$ the measured spindle speed in rpm and L the number of harmonics under consideration.

In the case of milling, the periodic movement of the cutter can be modeled as an input-output relation between the spindle-speed

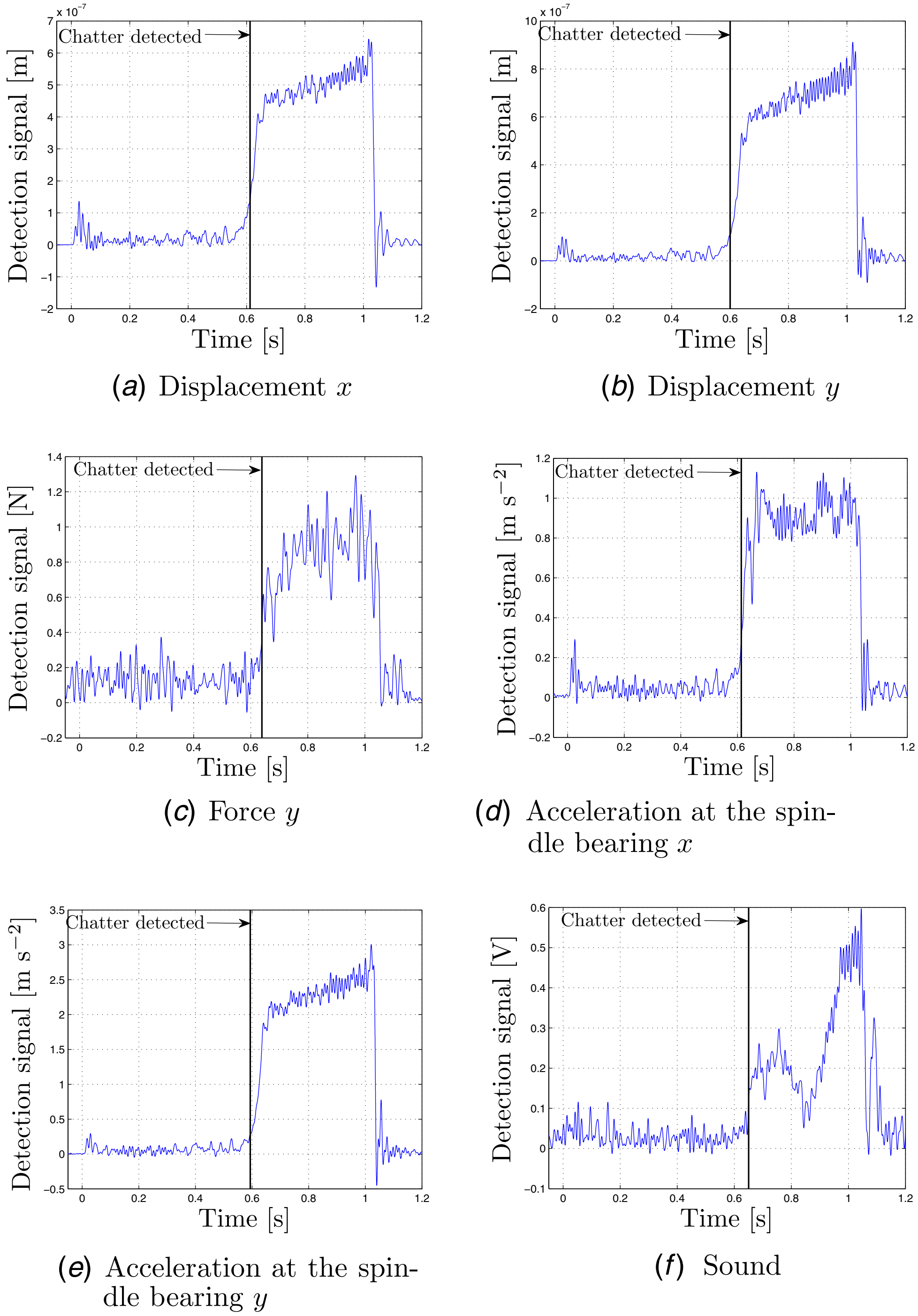

Fig. 5 Detection using various sensors

related perturbation $u_{\text{ref}}(k)$ and $a_p(k)$ without any dynamics, i.e., $F(q)=1$ in Eq. (8). The model of the periodic part can therefore be considered as a moving average (MA) process. As described in Sec. 2, when chatter occurs, the frequency spectrum consists of spindle speed and chatter frequencies. The chatter frequencies close to the machine spindle resonance will have a significantly larger amplitude than the other chatter frequencies (see Fig. 4(*b*), where the dominant chatter frequency lies around 2200 Hz). Therefore, the signal model of the perturbation part $a_u(k)$ can be considered as a so-called *narrow-band signal* of which the frequency and amplitude may vary in time. Commonly, a narrow-band signal can be modeled as an autoregressive moving average (ARMA) process. Since we are interested in the resonance (frequency and amplitude) of the model, which is modeled as a time-varying autoregressive (AR) signal model, we take $C(q)=1$ in Eq. (8). Taking the considerations stated above into account, the total signal model can be given as

$$a(k) = \sum_{l=1}^{L} B^l(q)u^l(k) + \frac{1}{D(q)}e(k) \tag{10}$$

where the polynomial $B^l(q)$ is defined as

$$B^l(q) = \left[B^l_{\cos}(q), B^l_{\sin}(q)\right] \tag{11}$$

Since the chatter vibrations are modeled by $D(q)$, it is expected that properties of $D(q)$ will predict the onset of chatter.

3.2.2 Identification of the Parametric Milling Model. The rational transfer functions $B^l(q)$ and $D(q)$ in Eq. (8) are unknown and are to be determined with an estimation procedure. The unknown coefficients of $B^l(q)$ and $D(q)$ are gathered in the parameter vector θ, i.e., $B^l(q,\theta)$ and $D(q,\theta)$. The one-step ahead predictor for the parametric milling model in Eq. (10) is given as

$$\hat{a}(k|\theta) = D(q,\theta)\sum_{l=1}^{L} B^l(q,\theta)u^l(k) + (1 - D(q,\theta))a(k) \tag{12}$$

The prediction error is defined as the difference between the measured and the predicted acceleration:

$$f_m(k,\theta) \coloneqq a(k) - \hat{a}(k|\theta) = D(q,\theta)\varepsilon(k,\theta) \tag{13}$$

with

$$\varepsilon(k,\theta) \coloneqq a(k) - \hat{a}_p(k) = a(k) - \sum_{l=1}^{L} B^l(q,\theta)u^l(k) \tag{14}$$

The two transfer functions $B^l(q,\theta)$ and $D(q,\theta)$ can be estimated independently as will be shown below. This is desirable, first, to reduce the complexities of the one-step-ahead prediction and, second, from a computational point of view. Hereto, the parameter vector θ is decomposed into two separate vectors, θ_p for the periodic transfer functions $B^l(q,\theta_p)$ and θ_u for the perturbation transfer function $D(q,\theta_u)$, i.e., $\theta = [\theta_p^T, \theta_u^T]^T$.

The first prediction scheme estimates the periodic part of the accelerations:

$$\hat{a}_p(k,\theta_p) = \sum_{l=1}^{L} B^l(q,\theta_p)u^l(k) \tag{15}$$

with cost function $J_p(\theta_p) = E[\varepsilon^2(k,\theta_p)]$, where $E[.]$ denotes the expectation operator. The second prediction scheme estimates the perturbation part of the measured accelerations:

$$\hat{a}_u(k,\theta_u) = \hat{a}(k|\theta) - \hat{a}_p(k|\theta_p) = (1 - D(q,\theta_u))\varepsilon(k) =: \hat{\varepsilon}(k,\theta_u) \tag{16}$$

with cost function $J_u(\theta_u) = E[(\varepsilon(k,\theta_p) - \hat{\varepsilon}(k,\theta_u))^2]$. Note that $J_u(\theta_u) = E[f_m^2(k,\theta)]$. Furthermore, note that by minimizing $J_p(\theta_p)$, we aim to minimize ε^2, which reflects the quality of the estimated $a_p(k)$ of the spindle-speed related accelerations. Moreover, the minimization of J_u, i.e., of $(\varepsilon(k,\theta_p) - \hat{\varepsilon}(k,\theta_u))^2 = f_m(k)^2 = (a(k) - \hat{a}(k,\theta))^2$, aims at good prediction of the overall acceleration signal.

The two-step prediction scheme approach, outlined above, may only be applied when the estimated signals $\hat{a}_p(k)$ and $\hat{a}_u(k)$ fulfill the property of orthogonality and have zero mean. Hereto, consider the expected value of the estimated signals to be defined as follows:

$$E\left[\begin{bmatrix} \hat{a}_p(k,\theta_p) \\ 1 \end{bmatrix} \hat{a}_u(k-\beta,\theta_u)\right] = \begin{bmatrix} \sigma_{pu}^2\delta(\beta) \\ 0 \end{bmatrix} \tag{17}$$

with covariance σ_{pu}^2, β the time shift operator, and $\delta(\beta)=1$ for $\beta=0$ and $\delta(\beta)=0$ for $\beta \neq 0$. For the property of orthogonality to hold, in practice, we require that $\sigma_{pu}^2 \ll 1$. To show that this is indeed the case, Eqs. (15) and (16) are substituted into Eq. (17), which gives

$$E\left[\begin{bmatrix} \sum_{l=1}^{L} B^l(q,\theta_p)u^l(k) \\ 1 \end{bmatrix} \hat{\varepsilon}(k-\beta,\theta_u)\right] = \begin{bmatrix} \sigma_{pu}^2\delta(\beta) \\ 0 \end{bmatrix} \tag{18}$$

From the definition of the input vector $u^l(k)$ in Eq. (9) and $\hat{a}_p(k)$ in Eq. (15), it is clear that the first prediction scheme estimates the periodic movement of the cutter at specific (spindle-speed related) frequencies. From Fourier theory, it is known that sinusoidal signals with different frequencies fulfill the orthogonality property, i.e., $\int_{t_0}^{t_0+2\pi/(Z\omega)} \sin(\omega t)\cos(2\omega t)dt = 0$. Generally, the (dominant) chatter frequency, which largely determines $\hat{a}_u(k)$, differs from the spindle-speed related frequencies. Hence, we can conclude that, in practice, $\sigma_{pu}^2 \ll 1$ and $a_p(k)$ and $a_u(k)$ can be estimated independently. When no chatter occurs, the estimation error of the first prediction scheme will, in theory, be equal to white noise. Then our assumption that the perturbation signal is a narrow-band signal does not hold. However, as will be shown in the experimental results in Sec. 5, in practice, the regenerative effect is already visible during stable cutting and, therefore, the assumption that the perturbation signal is a narrow-band signal still holds when no chatter occurs.

The problem now is to find parameter vectors θ_p, θ_u in Eqs. (15) and (16) such that the prediction error $f_m(k,\theta)$ is minimized.[2] The optimally estimated parameter vectors θ_p^o and θ_u^o are defined as, $\theta_p^o = \arg\min J_p(\theta_p)$ and $\theta_u^o = \arg\min J_u(\theta_u)$.

To solve the estimation problem, normally a set of measurement data is collected. These data are then processed off-line, using e.g., a least squares estimator. This off-line approach cannot be used for the chatter control system proposed for three reasons. First, knowledge on the state of the system (i.e., stable/unstable) is required at each time instant in order to detect chatter in an online and real-time fashion. Second, from the estimation parameters θ_u, the chatter frequency will be estimated, which is necessary for the control design that will be presented in Sec. 4. Third, the properties of the milling process may vary during the milling operation. Moreover, during a control action the spindle-speed changes, which results in a change of the milling process.

Section 3.2.3 describes the identification procedure that is able to deal with the time-varying properties of the milling process and that can be implemented in real time.

3.2.3 Recursive Identification of the Parametric Milling Model. Adaptive and recursive identification methods are designed to deal with the time-varying characteristics of dynamic processes (such as the milling process) and can be implemented in real time. To cope with the time-varying regenerative process and to be able to track variations in the process properties, an adaptive and recursive identification method is used to obtain parameter vectors θ_p^o and θ_u^o such that the cost functions $J_p(\theta_p)$ and $J_u(\theta_u)$ are minimized.

A major drawback of the use of recursive methods are the asymptotic properties of the estimation parameters. For fast changing time-variant systems, these drawbacks have disturbing side effects on the convergence time of an algorithm. The condition of orthogonality (18) may be violated, resulting in biased estimation of $B^l(q,\theta)$ and $D(q,\theta)$. Therefore, it is crucial to select an algorithm with excellent convergence and tracking properties.

The first prediction scheme is solved by application of the widely used normalized least mean squares (NLMS) algorithm. The NLMS algorithm is known because of its simplicity and ease of computation [23].

The NLMS algorithm is given by

$$\theta_p(k+1) = \lambda\theta_p(k) + 2\mu\frac{\varphi_p(k)\varepsilon(k)}{\|\varphi_p(k)\|^2} \tag{19a}$$

$$\varepsilon(k) = a(k) - \varphi_p(k)^T\theta_p(k) \tag{19b}$$

$$\varphi_p(k) = [u^1(k)^T, u^2(k)^T, \ldots, u^L(k)^T]^T \tag{19c}$$

$$\theta_p(k) = [B^1, B^2, \ldots, B^L]^T \tag{19d}$$

with $\theta_p(0)=0$, $u^l(k)$, and B^l as defined by Eqs. (9) and (11), respectively. Moreover, λ is the so-called forgetting factor, which resembles exponential windowing of the data. Without the forgetting factor, the algorithm is only able to track slow-varying prop-

[2]Note that the minimization of ε^2 in $J_p(\theta_p) = E[\varepsilon^2(k,\theta_p)]$ is only an intermediate step in the estimation process.

erties in the process. Typical values for λ lie in the range $\lambda \in [0.95, 0.9999]$. The step size is denoted with μ. The NLMS algorithm is convergent in the mean square if and only if $0 < \mu \leq 2$, see Ref. [23]. To prevent overshoot of the optimal solution, μ is normally chosen as $0 < \mu \leq 1$. Furthermore, the term $\|\varphi_p(k)\|^2$ will be constant when the spindle speed is constant, due to the fact that $\varphi_p(k)$ consists of sine and cosine series. However, in practice, the spindle speed is measured and will be changed during a control action. Therefore, $\|\varphi_p(k)\|^2$ will not be constant over the entire process and is computed recursively. The second prediction scheme can be written into a form that allows for the application of the Kalman filter. The state-space description of the Kalman filter is defined as follows:

$$x(k+1) = A(k)x(k) + v(k) \tag{20a}$$

$$y(k) = C(k)x(k) + w(k) \tag{20b}$$

with $x(0)=0$, $\Sigma_0 = E[x(0)x^T(0)]$, and $v(k)$ and $w(k)$ are assumed to be zero-mean Gaussian noise processes, which are uncorrelated with covariances and cross covariance defined by

$$E\begin{bmatrix} v(k) \\ w(k) \end{bmatrix}[v^T(k), w^T(k)] = \begin{bmatrix} R_v(k) & 0 \\ 0 & R_w(k) \end{bmatrix} \tag{21}$$

Furthermore, it its assumed that the noise processes $v(k), w(k)$ are uncorrelated with the initial state vector $x(0)$, i.e., $E[v(k)x^T(0)] = 0$ and $E[w(k)x^T(0)] = 0$. By taking $A(k)=I$, $C(k)=\varphi_u^T(k)$, $y(k) = \hat{a}_u(k) = \hat{\varepsilon}(k)$, $x(k) = \bar{\theta}_u(k)$ with $\bar{\theta}_u(k)$ the true parameter vector, and using the definition of $\hat{\varepsilon}(k)$ (see Eq. (16)), the state-space model (20) can be written as follows:

$$\bar{\theta}_u(k+1) = \bar{\theta}_u(k) + v(k) \tag{22a}$$

$$\hat{\varepsilon}(k) = -\varphi_u^T(k)\bar{\theta}_u(k) + w(k) \tag{22b}$$

with

$$\varphi_u(k) = [\varepsilon(k-1), \varepsilon(k-2), \ldots, \varepsilon(k-N_d)]^T \tag{23}$$

$$\bar{\theta}_u(k) = [\bar{d}_1, \bar{d}_2, \ldots, \bar{d}_{N_d}]^T \tag{24}$$

and N_d denotes the order of $D(q, \theta_u)$. N_d is typically set to 4 to be able to *monitor* two chatter frequencies. In this way, chatter frequencies related to either a structural mode or a tool mode can be determined. It should be noted that in the state-space description above the fact that $D(q, \theta_u)$ is a monic transfer function is used.

The Kalman filter based on the one-step prediction can be written as follows [24]: Given observation $\varepsilon(k)$ that satisfies the state-space model in Eq. (22), the identification process can be recursively solved by repeating for $k \geq 0$:

$$T(k) = P(k-1)\varphi_u(k) \tag{25a}$$

$$K(k) = T(k)(\varphi_u^T(k)T(k) + R_w(k))^{-1} \tag{25b}$$

$$f_m(k) = \varepsilon(k) - \varphi_u^T(k)\theta_u(k) \tag{25c}$$

$$\theta_u(k+1) = \theta_u(k) + K(k)f_m(k) \tag{25d}$$

$$P(k) = P(k-1) + R_v(k) - K(k)\{R_w(k) + \varphi_u(k)T(k)\}K^T(k) \tag{25e}$$

with initial conditions $\theta_u(0)=0$ and $P(0)=\Sigma_0$. The convergence rate and tracking properties of the estimation can be tuned with the appropriate values for R_v and R_w. In this particular application, these parameters are kept constant during the identification procedure. The values of the four tunable parameters, μ, λ, R_v, and R_w, are determined experimentally.

3.2.4 Detection of Onset of Chatter. As discussed above, the properties of $\hat{a}_u(k)$ will predict the onset of chatter since $\hat{a}_u(k)$ reflects the signal content of the measured acceleration signal not related to the spindle speed. Therefore, the detection of onset of chatter is now transformed into the determination of the state of the time-varying autoregressive signal model $\hat{a}_u(k) = (1 - D(q, \theta_u))\varepsilon(k)$, i.e., the model of the perturbation part. Hence, the detection criterion should indicate the time-varying *strength* of the estimated perturbation signal $\hat{a}_u(k, \theta_u)$. Two commonly used chatter detection criteria in the case of parametric modeling are either based on the roots $\underline{\alpha}$ of $D(q, \theta_u)$ or the peak value of the power spectral density (PSD) function, see Ref. [20]. Since the peak value of the PSD function is located at the dominant chatter frequency, the value can be calculated directly,

$$H(f_{\text{chat}}(k), \theta_u) = \left|\frac{1}{D(q, f_{\text{chat}}(k))}\right|^2 = \left|\frac{1}{1 + \sum_{n=1}^{N_d} d_n(k)e^{-i2\pi f_{\text{chat}}(k)nT_s}}\right|^2 \tag{26}$$

The dominant chatter frequency f_{chat} is estimated from the dominant root $\bar{\alpha}$ of $D(q, \theta_u)$ by

$$f_{\text{chat}}(k) = \text{Im}\left(\frac{\ln(\bar{\alpha})}{2\pi}F_s\right) \tag{27}$$

where $F_s = 1/T_s$ denotes the sampling frequency. In the case of chatter, the identification results of the milling model will be biased and the estimated transfer function $D(q, \theta_u)$ will be unstable (i.e., $|\bar{\alpha}| > 1$). This results in an unreliable reconstruction of $\hat{a}_u(k)$. One way to prevent this unstable identification process is to reflect the unstable roots with the unit circle. The reflected distance to the unit circle can be defined arbitrarily. Here, a distance of $\delta = 0.001$ to the unit circle is chosen.

Here, a third criterion for chatter detection will be considered, namely, the variance of the perturbation part of the measured acceleration (16). The variance is calculated from the estimation error $\varepsilon(k)$ of the first prediction scheme, i.e., $\sigma_\varepsilon^2 = E[\varepsilon^2(k)]$. It is expected that the three detection criteria (dominant root $\bar{\alpha}$ of $D(q, \theta_u)$, the PSD value at the chatter frequency f_{chat}, and the variance of the perturbation part σ_ε^2) will perform differently for an unstable milling process but comparable for a stable milling process. The choice of which detection criterion to use will be based on experimental results with the detection algorithm, which are presented in Sec. 5.

4 Chatter Control

Basically three methods exist to overcome or avoid chatter, namely, continuous spindle-speed variation, passively or actively altering the machine dynamics and adjusting the spindle speed. In this work, we use the strategy to adjust the spindle speed and feed to avoid chatter. This method can be implemented on a state-of-the-art high-speed milling machine, without any major changes to the machine, by using the feed override and spindle override functions of the machine. In this section, two methods are presented that automatically adjust the spindle speed in case (the onset of) chatter occurs. Hereto, the detection method of Sec. 3.2 is used. This method gives both an indication that (the onset of) chatter occurs and an estimation of the dominant chatter frequency.

In Fig. 6, a schematic representation of the closed loop including the milling process, chatter detection, and chatter control is depicted. An initial working point (spindle speed and depth of cut) is chosen by the machinist based on a model-based stability lobe diagram (SLD), see, e.g., Ref. [25], or practical experience. This working point is used in the NC program. During the milling process, this spindle speed is maintained as long as (the onset of) chatter is not detected using the detection method presented in Sec. 3.2. When (the onset of) chatter is detected, a new spindle-speed setpoint is computed and sent to the HSM machine using the spindle-speed override function. In the same time, the feed is adapted to ensure a constant feed per tooth.

The detection method gives an indication whether or not (the onset of) chatter occurs. Furthermore, the dominant chatter fre-

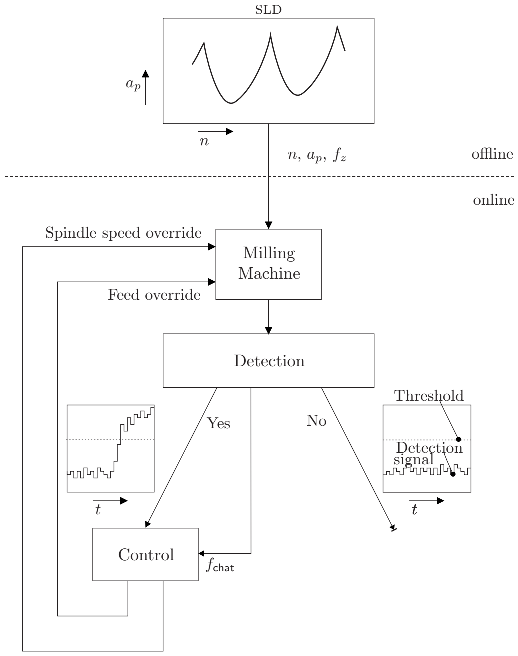

Fig. 6 Schematic representation of the closed loop including the milling process, chatter detection, and chatter control

quency f_{chat} is computed. This chatter frequency is used to compute a new spindle-speed setpoint in a chatter-free zone in the case (the onset of) chatter occurs. Hereto, also the actual spindle speed should be known since it is needed in the detection method and, as will be shown below, it is needed in the computation of the new spindle-speed setpoint. The new spindle-speed setpoint can be chosen based on two requirements, namely, robustness against chatter and lowering the perturbation vibrations of the cutter. The chatter controller, as depicted in Fig. 6, is basically a setpoint generator in closed loop with the HSM machine and the detection algorithm. The internal speed controller of the HSM machine is used to control the spindle speed to its setpoint. In Sec. 4.1, a control strategy is presented that focuses on robustness against chatter, whereas Sec. 4.2 presents a control strategy that lowers the perturbation vibrations of the cutter and at the same time guarantees a robust milling performance.

4.1 Control Strategy 1. In the first control strategy, a new spindle speed is chosen such that the estimated dominant chatter frequency f_{chat} coincides with a (higher harmonic of) the new tooth pass excitation frequency f_{TPE}.

The chatter frequency is related to the phase difference between two subsequent waves by [26]

$$\epsilon + p = f_{chat}(k)\frac{60}{Z\Omega(k)} \tag{28}$$

with p the (integer) lobe number, ϵ the fraction of incomplete waves between two subsequent cuts, and $\Omega(k)$ the measured current spindle speed in rpm. The new spindle speed is computed such that $\epsilon=0$, see Ref. [3]. Hereto, first the new lobe number is computed by

$$p_{new}(k) = \left\{\frac{60 f_{chat}(k)}{Z\Omega(k)}\right\} \tag{29}$$

where $\{.\}$ means rounding toward the nearest integer. The new spindle speed is then computed by

$$\Omega_{new}(k) = \frac{60 f_{chat}(k)}{p_{new}(k) Z} \tag{30}$$

Using this method, the spindle speed is directed toward the center of the lobe. However, the exact center of the lobe may not be characterized by Eq. (30). As mentioned in Ref. [27], if the initial working point is in the lower part of a lobe, the new setpoint lies near the center of the lobe. However, in the peak of the lobe, $\Omega_{new}(k)$ as in Eq. (30) is generally not (exactly) at the center of the lobe and, consequently, it may happen that the new setpoint may cross the next lobe.

When the spindle speed is changed, this will lead to a new chatter frequency and, hence, the setpoint is changed accordingly. Therefore, the setpoint will be updated constantly as long as the cut is being marked as exhibiting chatter. When the cut is marked as not exhibiting chatter, the most recent computed setpoint is maintained. Therefore, the spindle speed can still change although chatter has already been eliminated. The benefit of this method is the fact that the spindle speed moves further toward the center of a stable area of the SLD if the lobes are wide. If the lobes are narrow (e.g., in the peak of a lobe), another strategy is to change the setpoint to the actual spindle speed when chatter is eliminated. This may prevent overshoot in the case of narrow lobes. In this work, we use the first strategy and leave alternatives for future work.

4.2 Control Strategy 2. The first control strategy, presented in Sec. 4.1, avoids chatter occurrence by setting the tooth-passing frequency equal to the chatter frequency resulting in a zero phase difference ϵ between two subsequent teeth motions. While this approach is robust for changes in the milling process, no guarantees can be given for the performance in terms of the level of vibrations of the process. Therefore, we propose a second control strategy with the goal to lower the total perturbation vibrations $a_u(k)$ and maintain robustness of performance by adapting the spindle speed and feed. This strategy is known as extremum seeking control and generally no guarantees can be given on whether a global minimum is found.

Essential in the development of this second control strategy is the existence of a deterministic relation between perturbation vibrations and the spindle speed. Moreover, the relation between perturbation vibration and parameters of the milling process parameters, such as spindle speed, depth-of-cut, and feed rate, is necessary to design a suitable controller. In general, no exact disturbance model can be found that analytically describes the relation between perturbation vibration and parameters of the milling process. Therefore, this relation is determined empirically. Hereto, milling experiments at a Mikron 700 HSM are performed for several spindle speeds Ω at a constant depth of cut of $a_p=3.5$ mm and feed per tooth $f_z=0.2$ mm/tooth. The acceleration is measured during the cut using an accelerometer, which is mounted near the lower spindle bearing. The measured accelerations are processed off-line using a MATLAB/SIMULINK implementation of the detection method presented in Sec. 3. Figure 7 presents the resulting relation of the perturbation vibration, measured via the PSD $H(f_{chat}(k),\theta_u)$ of $D(q,\theta_u)$ at the chatter frequency, which is presented in Sec. 3.2.4, as function of the spindle speed for one specific set of depth of cut and feed per tooth. In the same figure, the difference between the estimated dominant chatter frequency $f_{chat}(k)$ and the coinciding higher harmonic of the tooth-passing frequency, defined as $p_{new}(k)f_{TPE}$, with $p_{new}(k)$ as in Eq. (29). The difference is denoted as $\Delta f(k)=f_{chat}(k)-p_{new}(k)f_{TPE}$. From the figure, it can be seen that in the first control strategy, presented in Sec. 4.1, the point where Δf crosses the zero axis is calculated (in this case, $\Omega_{new}=33{,}000$ rpm). For the second control strategy, the minimum value of the empirically obtained function should be found resulting in a new spindle-speed setpoint of $\Omega_{new}=33{,}600$ rpm. Both spindle setpoints are positioned relatively close to each other, which implies that lowering the perturbation

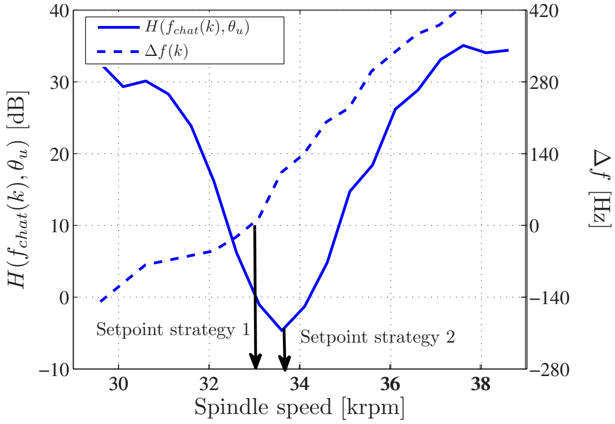

Fig. 7 Power spectral density $H(f_{\text{chat}}(k),\theta_u)$ (solid) and $\Delta f(k)$ (dashed) based on measured accelerations for a spindle-speed sweep from 29,600 rpm to 38,600 rpm at a constant depth of cut

vibrations will also result in robust chatter prevention. The minimum value of the objective function, as given in Fig. 7, will be determined via an extremum seeking control-like algorithm, which will be described Sec. 4.2.1.

4.2.1 Control Design. As outlined above, no analytical relation can be found between the spindle speed and the perturbation vibrations. Therefore, the controller will continuously try to lower the estimated perturbation vibrations of the mill by adapting the spindle speed. The controller will therefore utilize a feedback control scheme to determine the optimal spindle speed that coincides with the minimum value of $H(f_{\text{chat}}(k),\theta_u)$ defined in Eq. (26). The feedback signal is therefore $H(f_{\text{chat}}(k),\theta_u)$. The inputs of the controller are the initial spindle-speed setpoint Ω_0, the PSD $H(f_{\text{chat}}(k),\theta_u)$ of $D(q,\theta_u)$ and the dominant chatter frequency $f_{\text{chat}}(k)$. The controller output is the new spindle-speed setpoint $\Omega_{\text{new}}(k)$. The spindle-speed trajectory is calculated according to

$$\Omega_{\text{new}}(k)=\Omega_0(1+\theta_c(k)) \tag{31}$$

where $\Omega_{\text{new}}\in[\Omega_{\min},\Omega_{\max}]$, $\theta_c\in\mathbb{R}$, and Ω_0 is the initial spindle speed, $\theta_c(k)$ is the controller parameter and where $\Omega_{\min}$ and $\Omega_{\max}$ represent the minimum and maximum spindle speeds of a milling machine. The control objective is to minimize the predefined cost function $J_c(\theta_c)$, defined by $J_c(\theta_c)=E[H(f_{\text{chat}}(k),\theta_u)]$, as function of θ_c. From Fig. 7, the selected cost function $J_c(\theta_c)$, as function of the spindle speed, has a (dominant) parabolic shape with a global minimum within one lobe. It is therefore plausible to consider the determination of the minimum value of the cost function with respect to $\theta_c(k)$ as an identification problem and evidently the optimal value for the parameter θ_c (and thus also for Ω) is defined as $\theta_c^o=\arg\min J_c(\theta_c)$. To automatically obtain the optimal θ_c^o at which the cost function has a minimum value, the well-known NLMS algorithm [23] is used. The properties of the NLMS algorithm are already outlined in Sec. 3.2.3. The control algorithm is given by Eq. (31) with

$$\theta_c(k+1)=\theta_c(k)-2\mu_c\frac{\sqrt{\bar{H}}}{|\gamma(k)|}\text{sign}(\Delta f(k)) \tag{32}$$

where $\bar{H}:=H(f_{\text{chat}}(k),\theta_u)$, $\Delta f(k)=f_{\text{chat}}(k)-p_{\text{new}}(k)f_{\text{TPE}}(k)$, with initial condition $\theta_c(0)=0$, and $\gamma(k)$ the exponential moving average of $\sqrt{H(f_{\text{chat}}(k),\theta_u)}$ given by

$$\gamma(k)=(1-\lambda_c)\gamma(k-1)+\lambda_c H(f_{\text{chat}}(k),\theta_u) \tag{33}$$

with initial condition $\gamma(0)=0$, λ_c the smoothing factor, μ_c a tunable parameter that determines the step size, $H(f_{\text{chat}}(k),\theta_u)$ the time-varying PSD of $D^{-1}(q,\theta_u)$ at the chatter frequency $f_{\text{chat}}(k)$

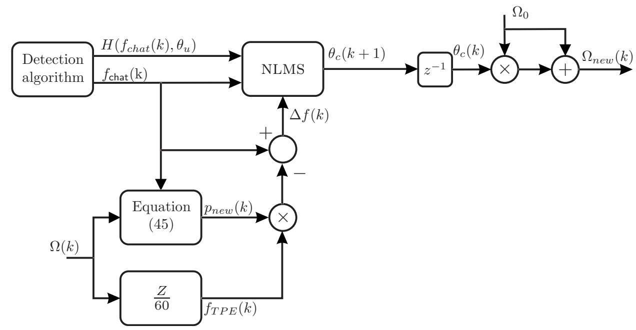

Fig. 8 Schematic overview of the adaptive chatter controller

(see Eq. (26)) and $p_{\text{new}}(k)$ as defined in Eq. (29). A schematic overview of the proposed controller is given in Fig. 8.

4.3 Properties of the Control Strategies. The control strategy outlined in Sec. 4.1 calculates a new spindle setpoint and overrides the internal controller of the milling without any feedback mechanism to measure the performance of the milling process. The new setpoint will introduce a stepwise change in the setpoint for the HSM's spindle-speed controller and the performance will therefore strongly depend on the internal spindle-speed controllers of the HSM and the dynamic behavior of the closed-loop spindle system. We note that the HSM milling machine has suitable internal controllers and an optimized trajectory generator.

The main objective of the control strategy outlined in Sec. 4.2 is to lower the perturbation vibrations by finding the optimal spindle speed. The adaptive proportional controller calculates iteratively the optimal spindle-speed trajectory using a feedback scheme. In fact, the algorithm represents a trajectory generator for the HSM's spindle-speed controller. The control parameters μ_c and λ_c should be tuned such that the controller is insensitive for time delay in the HSM's control system. The parameter values have to be tuned during the experiments. For varying time delays in the machine control system, the value of μ_c should chosen quite conservatively (i.e., $\mu_c<1$), which can lead to deterioration in the settling time of the control action.

5 Experiments

Experiments have been performed to test the detection and control method in practice. All experiments are performed on a Mikron HSM 700 milling machine. The acceleration is measured at the nonrotating part of the spindle near the lower spindle bearing using an accelerometer, type Brüel & Kjær 4382. The detection and control algorithms are implemented on a dSpace system with a sample time of $T_s=1\times10^{-4}$ s. The parameters of the recursive identification algorithms, described in Sec. 3, determined for the experiments are listed in Table 1. All cuts have been made in aluminum 6082 using a Jabro Tools JH421 cutter (two flute cutter with a diameter of 10 mm and length of 57 mm) mounted in a Kelch HSK40 shrink-fit holder. First, experiments are performed to validate the detection method experimentally. Second, experimental results for the two control strategies are presented.

5.1 Detection. Experiments have been performed to validate the detection method experimentally. First, a detection signal has

Table 1 Parameters of the identification algorithms given by Eqs. (19) and (25)

μ	λ	R_v	R_w
0.5	0.9995	3×10^{-5}	8×10^{-4}

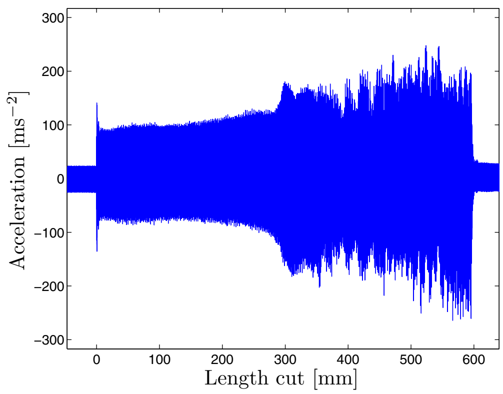

(*a*) Acceleration

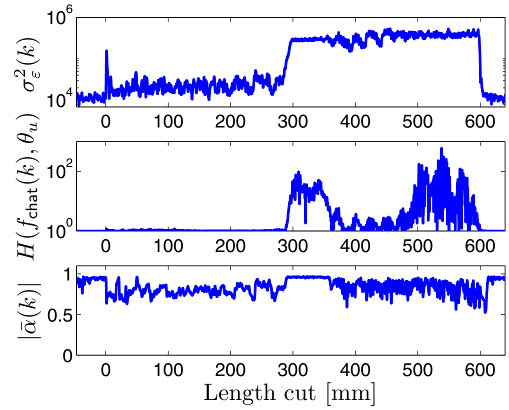

(*b*) Detection criteria

Fig. 9 Experimental results of chatter detection method. Chatter is first detected after 288 mm.

to be selected. In Sec. 3.2.4, three possible detection criteria were described, namely, (1) variance of the estimation error of the first prediction scheme $\sigma_\varepsilon^2(k)$, (2) $H(f_{\text{chat}}(k),\theta_u)$, the PSD of $D^{-1}(q,\theta_u)$ at the dominant chatter frequency $f_{\text{chat}}(k)$, and (3) the absolute value of the dominant root $\bar{\alpha}(k)$ of $D(q,\theta_u)$.

The outcome of the detection criteria are compared with the surface of the workpiece.

A full immersion cut has been made at a spindle speed of 35,000 rpm where the axial depth of cut increases from 2.0 to 3.0 mm over a length of 600 mm, which results in the occurrence of chatter during the cut. In Fig. 9, the acceleration measured at the lower spindle bearing and the three detection criteria are depicted. From Fig. 9(*b*), it can be seen that the variance $\sigma_\varepsilon^2(k)$ increases upon tool entering. The entering of a tool in the material can be seen as an impulse excitation in the force acting on the tip of the mill. This implies that next to spindle-speed frequencies also other frequencies are present in the acceleration signal. These other frequencies are not predicted by the first prediction scheme and therefore the estimation error of the first prediction scheme $\varepsilon(k)$ increases. After tool impact the variance decreases again. At approximately 288 mm, a significant increase is seen in the variance. By inspection of the workpiece, see Fig. 11, it can be seen that the first chatter marks are visible around 293 mm. Hence, the increase in the detection signal indicates the occurrence of onset of chatter, as is expected. The variance of the estimation error of the first prediction scheme does not decrease and holds approximately the same value, which reflects the marks seen on the workpiece surface, indicating the occurrence of (onset of) chatter.

When considering the second detection criterion, i.e., the PSD function $H(f_{\text{chat}}(k),\theta_u)$ at the dominant chatter frequency, no significant increase in the detection signal is seen upon tool entering. This can be clarified by realizing that the detection signal is calculated at a single frequency, i.e., the estimated dominant chatter frequency $f_{\text{chat}}(k)$. As with the first detection criterion, a significant increase in the detection criterion is seen at approximately 288 mm indicating the onset of chatter as described above. However, after this increase, a subsequent decrease in the detection signal occurs. This can be explained as follows. By further increasing the depth of cut, the milling process becomes unstable and shows nonlinear behavior. This implies that the roots of the estimated perturbation model will move further away from the unit circle resulting in a decrease in $H(f_{\text{chat}}(k),\theta_u)$. So, after the detection signal crosses a user-defined threshold and chatter is said to occur, the signal will become smaller than the threshold and chatter is no longer detected. This is not in agreement with the marks on the workpiece, as can be seen in Fig. 11.

The third detection criterion, i.e., the absolute value of the dominant root $\bar{\alpha}(k)$ of $D(q,\theta_u)$, $|\bar{\alpha}(k)|$ varies between 0 and 1. Before tool entering, the criterion value lies close to 1, indicating that the system is close to instability. However, this is not the case, since the tool is not yet in cut. When the rotating tool is not in cut, only spindle-speed related frequencies are present in the acceleration signal. These are filtered out by the first prediction scheme. Therefore, the perturbation signal is a broad-band signal and the assumption that the regenerative effect is a narrow-band signal does not hold. When the tool enters the material, a drop in the detection signal, $|\bar{\alpha}(k)|$, is seen. This can be explained by realizing that in practice the regenerative process already influences the acceleration spectrum. The fact that this is indeed the case is visualized in the spectrogram in Fig. 10, where the Fourier transform of $a(k)$ is given as function of the cutting length. It can be seen that already an extra frequency, i.e., a frequency that does not coincide with a spindle-speed related frequency, is present in the acceleration signal just after tool impact, although this frequency is very small in amplitude. Hence, the perturbation signal $a_u(k)$ is a narrow-band signal and the detection algorithm is able to estimate the perturbation motions. As in the other two detection criteria, at approximately 288 mm a (small) increase is seen in the detection criterion. Although the dominant root $|\bar{\alpha}(k)|$ shows an increase in amplitude during onset of chatter, the signal is noisy

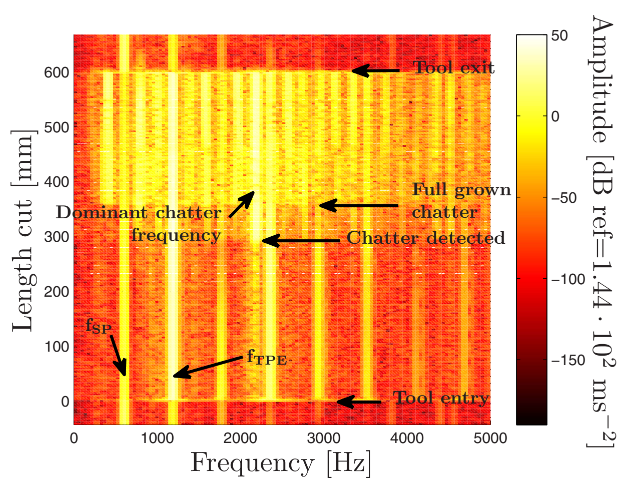

Fig. 10 Spectrogram of the measured acceleration at the lower spindle bearing for a cut without control. The brighter colors represent a larger magnitude of the frequency component.

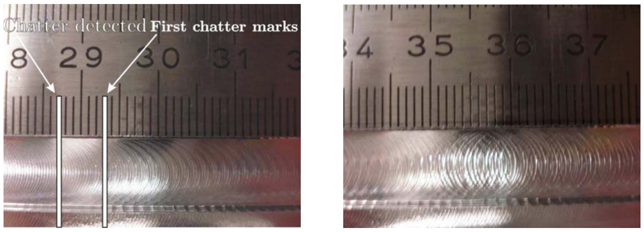

(*a*) from 280 to 320 mm

(*b*) from 340 to 375 mm

Fig. 11 Detail of the workpiece for a single cut without control at a spindle speed of 35,000 rpm with an increasing depth of cut from 2.0 mm to 3.0 mm

and it would not be easy to determine a robust detection threshold. When the depth of cut is further increased, the unstable poles of $D(q,\theta_u)$ are reflected inside the unit circle, as described in Sec. 3.2.4, which results in a decrease in the detection criterion.

Resuming, it can be said that all three criteria perform well in the case of a stable milling operation and, moreover, during onset of chatter. This justifies the application of the peak value of the PSD at the chatter frequency and the roots of $D(q,\theta_u)$ in the second control strategy that is presented in Sec. 4.2.

Based on the discussion above, the variance of the estimation error of the first prediction scheme, $\sigma_\varepsilon^2(k)$, is taken as detection signal. Although multiple criteria can be combined into one criterion, the single criterion (estimation error of the first prediction scheme) performed satisfactorily for all experiments. By setting the detection threshold to $\sigma_{\varepsilon,0}^2=6.678\times 10^4\ \mathrm{m}^2\ \mathrm{s}^{-4}$, chatter is detected after approximately 288 mm. For automatic control, it is desirable to select the threshold automatically. One way to do so would, for example, be to select the threshold based on amplitude of the first spindle-speed harmonic. The automatic selection of algorithm parameters is an extensive topic for further research and is therefore not considered here.

In Fig. 10, a spectrogram of the acceleration signal is shown. The spindle-speed and tooth-passing related frequencies can be clearly distinguished from the spectrogram. Furthermore, when chatter is detected after 288 mm, only the dominant chatter frequency is present in the frequency spectrum next to the spindle-speed related frequencies. At approximately 360 mm, chatter is fully grown. It can be seen that at that moment, all chatter frequencies are present in the frequency spectrum.

In Fig. 11, top views of the resulting workpiece are depicted. It can be seen that at the moment chatter is detected, no clear chatter marks are visible on the workpiece. The first (small) chatter marks appear at 293 mm. From Fig. 11(*b*), it can be seen that chatter is fully grown at 352 mm. Hence, it can be concluded that the results of the detection method in Fig. 9 coincide very well with the path that is left behind by the cutter. Furthermore, it can be seen that chatter is detected in a very early stage (even before chatter marks are visible on the workpiece).

5.2 Control. In order to apply the control strategies presented in Sec. 4, the hand terminal of the Mikron HSM 700 is modified such that the feed override and spindle-speed override can be controlled using an external electric potential. This means that the spindle speed can be changed within an interval ranging from 50% to 120% of the initial spindle speed Ω_0 and the feed can be modified within an interval ranging from 0% to 100% of the initial feed. Hence, using this particular setup, it is not possible to increase the spindle speed while maintaining a constant chip load. Therefore, when the spindle speed in increased, the chip load decreases with maximally 20%. Since the initial chip load is set to 0.2 mm/tooth, the minimal chip load is 0.16 mm/tooth, which is still sufficient for cutting aluminum. One major disadvantage of using the override as control input is the possibly large time delay between control input and actuation moment, due to a generally lower priority that is assigned to override control in the HSM's control system. For this typical milling machine, it is determined that the delay varies between 40 ms and 70 ms. The presence of such delay may adversely affect the control performance.

In Fig. 12, the results are depicted for a full immersion cut where the depth of cut is increased from 2.0 mm to 3.0 mm with an initial spindle speed of 35,000 rpm. The total path length is 600 mm, which is cut in about 2.6 s. In this way, the process is forced into an unstable region. This can be seen as a worst-case scenario, since the goal of the control strategy is to ensure chatter-free milling for relatively low-frequent, time-varying changes of the stability lobes diagram. The same cut is repeated two times. The first cut is performed using controller strategy 1 (Sec. 4.1), whereas the second cut is made using control strategy 2 (Sec. 4.2). The parameters for the second control strategy are chosen as $\mu_c=0.7$ and $\lambda_c=0.3$.

In the Figs. 12(*a*) and 12(*b*), the measured acceleration is depicted together with the (scaled) detection signal that shows whether or not chatter is detected. The sign of $\Delta f(k)=f_{\mathrm{chat}}(k)-p_{\mathrm{new}}(k)f_{\mathrm{TPE}}(k)$, indicates the direction in which the spindle speed should be changed. As can be seen, chatter is detected just before a major increase in the acceleration is observed. This implies that chatter is detected during onset and before the workpiece is damaged as is already shown in Sec. 5.1. The variance of $\varepsilon(k)$ is depicted in Figs. 12(*c*) and 12(*d*). The spindle speed and the spindle-speed setpoint provided by the controllers are shown in Figs. 12(*e*) and 12(*f*). When the variance exceeds the threshold, the cut is marked as exhibiting chatter. As described in Sec. 5.1, an increase in the detection signal $\sigma_\varepsilon^2(k)$ is seen when the tool enters the material. However, the response due to tool entering is damped out relatively fast and therefore no control action is induced. When chatter is detected, a new setpoint for the spindle speed is computed and sent to the spindle-speed override function of the hand terminal. In this particular case, a decrease in spindle speed is desired. It can be seen that the setpoint of the first control strategy overshoots the eventual setpoint. This is due to, first, delay in the control system and, second, the fact that the chatter frequency differs at different spindle speed. In order to prevent high-frequent oscillation of the setpoint, due to changes in $\mathrm{sign}(\Delta f(k))$, a low-pass filter is added to the estimated chatter frequency.

After the setpoint is reached, for both control strategies, the cut remains stable even when the depth of cut is increased further. It can be observed that it takes some time for the spindle speed to reach the setpoint. The settling time of the closed-loop spindle system is due to (1) delay in the controller of the Mikron HSM700 (typically between 40 ms and 70 ms) and (2) the large inertia of the spindle in combination with the standard spindle-speed controller of the Mikron HSM700, which is not specifically tuned for tracking relatively fast changes in spindle speed. The setpoint that is computed by control strategy 1 varies rapidly, as is depicted in Fig. 12(*e*). In order to decrease the variation in the setpoint, the cutoff frequency of the low-pass filter can be lowered. However, the actual spindle speed does not have these large variations due to the relatively low bandwidth of the closed-loop spindle system. The spindle speed is adjusted smoothly toward the chatter-free area. However, a mismatch between the setpoint and actual spindle speed for the second control strategy is seen. This is probably due to lack of integral control of the internal spindle-speed controller of the milling machine.

As can be seen in Fig. 12(*a*), the amplitude of the acceleration at the end of the cut is about $200\ \mathrm{m/s}^2$ in case control strategy 1 is chosen. For the case where the control strategy 2 is switched on, the amplitude of the acceleration is about $145\ \mathrm{m/s}^2$ (see Fig. 12(*b*)). When the controller is switched off, the acceleration signal is very noisy with spikes up to $260\ \mathrm{m/s}^2$ (see Fig. 9). Therefore, using the controller, the acceleration at the spindle bearing is decreased and is even further decreased when control strategy 2 is used (compare Figs. 12(*a*) and 12(*b*)). Although the amplitude of

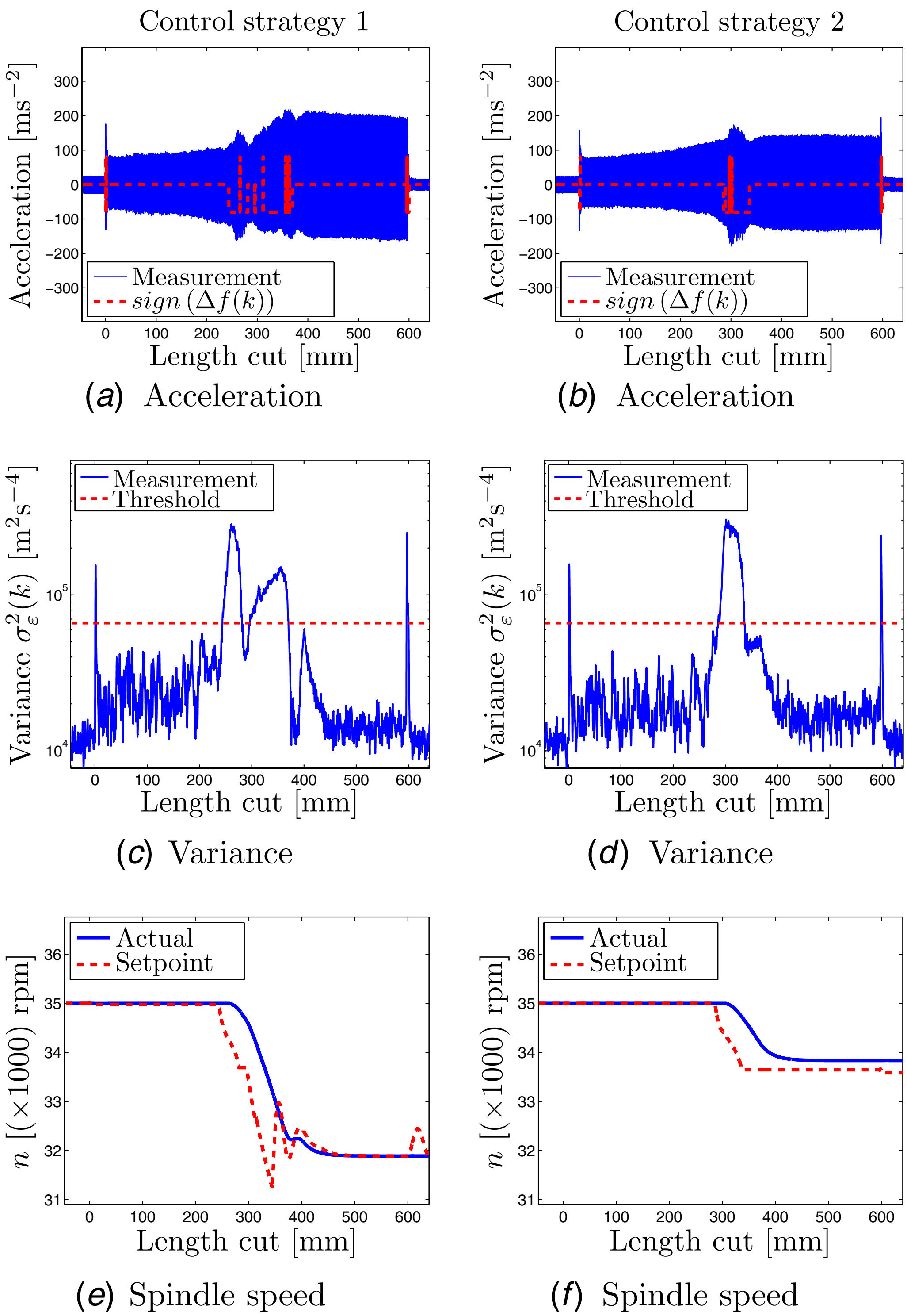

Fig. 12 Experimental results of the control strategies for a cut at 35000 rpm with increasing a_p from 2.0 mm to 3.0 mm in 2.6 s. (Left figures) Control strategy 1. (Right figures) Control strategy 2.

the accelerations with and without control do not differ that much, the frequency spectrum is totally different. This can be seen from Fig. 13, where the measured acceleration signal, for each control strategy, is shown in a spectrogram. In case the controller is switched off, the frequency spectrum consists of spindle-speed related frequencies and chatter frequencies, see Fig. 10. However, it can be clearly seen that no chatter frequencies are visible in the frequency spectrum of the acceleration in case the controllers are switched on. Moreover, by using control strategy 1, the second harmonic of the new tooth-passing frequency f_{TPE} is set to the dominant chatter frequency (which is clearly visible in Fig. 13(a)). From the spectrogram of the measured acceleration for the second control strategy (Fig. 13(b)), it can be seen that (a higher harmonic of) tooth-passing frequency does not coincide with the dominant chatter frequency.

In Fig. 14, the results, for the case where the controllers are switched on, are shown in the spindle-speed/depth-of-cut param-

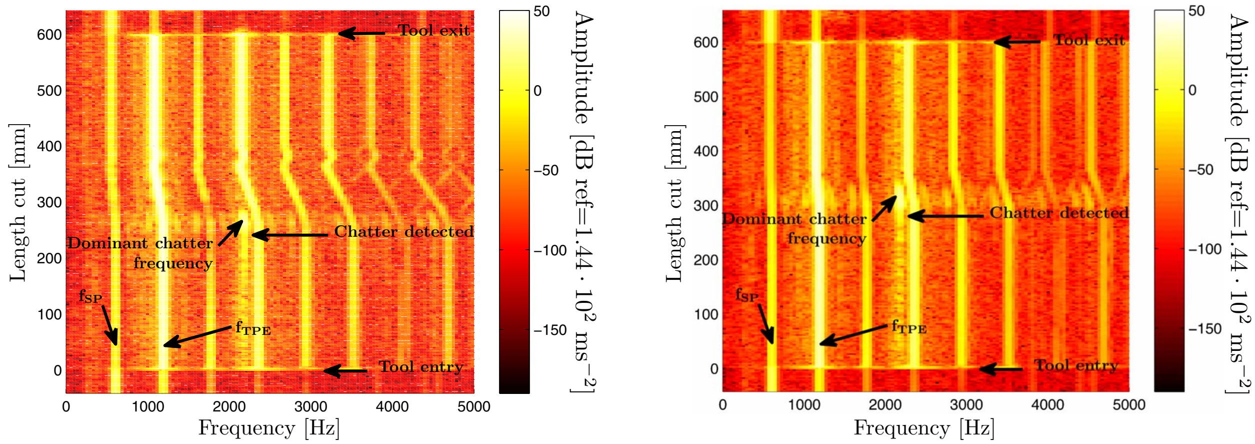

(*a*) Control strategy 1 (*b*) Control strategy 2

Fig. 13 Spectrogram of the acceleration measured at the lower spindle bearing for both control strategies

eter space. Here, the cut moves from a low to a higher value for the depth of cut. Moreover, chatter is indicated when the detection signal exceeds the defined threshold level. It can be seen that for both control strategies, the controller ensures that the working point moves away from instability and ensures a stable cut.

Pictures of a detail of the workpiece are shown in Fig. 15. For sake of clarity, also a picture of a cut with the controller switched off is shown. Clearly, when the controller is switched off, the wall of the workpiece is not smooth, whereas the wall of the workpiece remains smooth when the controller has been switched on. When the controller is switched on, no chatter marks can be seen on the workpiece after the setpoint has been reached. Furthermore, the spindle speed is changed, while the milling continues (i.e., the feed remains nonzero). If the feed would have been stopped, this would have led to a significant decrease in production time.

Hence, it can be concluded that the proposed control strategies work in practice. The control strategies ensure stable working points while the feed remains nonzero. Moreover, the detection and control algorithms are fast enough to be used at high spindle speeds.

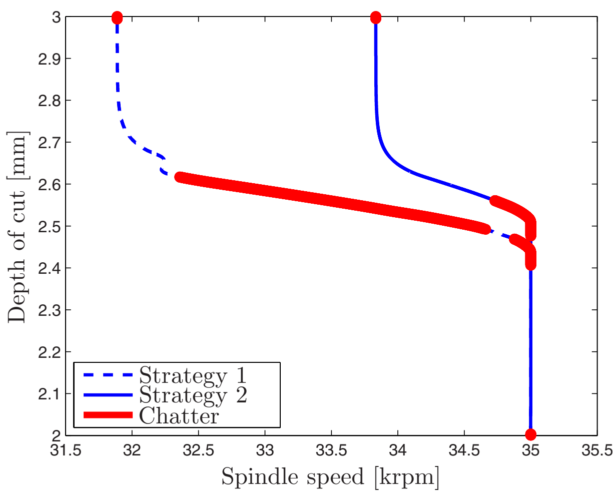

Fig. 14 Results of the experiments with the controllers switched on

6 Conclusions

In this paper, two control strategies are presented that guarantee chatter-free high-speed milling operations by automatic adaptation of spindle speed and feed (i.e., the feed is not stopped during the spindle-speed transition). In this way, the high-speed milling process will remain stable despite changes in the process, e.g., due to heating of the spindle and tool wear. The first control strategy eliminates chatter by setting the tooth-passing frequency equal to the dominant chatter frequency. The goal of the second chatter control strategy is to minimize the total chatter vibrations by spindle-speed adaptation. For both control strategies, an accurate and robust chatter detection algorithm is required. Therefore, this paper presents a novel chatter detection algorithm that automatically detects chatter in an online fashion and in a premature stage, such that no chatter marks are visible on the workpiece yet. Experimental results show that by using the control strategies chatter-free machining is ensured. It is shown that the detection algorithm is indeed able to detect chatter before it is fully developed. Furthermore, both control strategies ensure that chatter is avoided, thereby ensuring robust and high surface quality. Furthermore, where the first control strategy only ensures the avoidance of chatter, the second control strategy also lowers the chatter vibrations.


(*a*) Control off (*b*) Control strategy 1 (*c*) Control strategy 2

Fig. 15 Detail of the workpiece with and without chatter control. The depth of cut is increasing from 2.0 mm to 3.0 mm and the spindle speed is 35,000 rpm.

To improve the results even further, first, the control action should be introduced directly to the internal spindle-speed controller of the HSM, instead of via the hand terminal, such that the delay in the controller is minimized. Second, the internal spindle-speed controller of the HSM should be tuned properly, to be able to improve the tracking of the desired spindle-speed setpoints.

Moreover, the tuning of the presented detection and control strategy is machine specific. To even further enhance practical applicability (for entire machine parks), we foresee that automatic tuning, exploiting recent work on identification methods based on recursive lattice predictors as presented in Ref. [28], will be beneficial.

Finally, while in this paper the chatter detection procedure is used for chatter control purposes, the strategy can also be used for the efficient, in-process experimental determination of stability lobe diagrams. In this way, the effect of modeling inaccuracies in the milling model on model-based stability lobe diagrams can be overcome.

References

[1] Wiercigroch, M., and Budak, E., 2001, "Sources of Nonlinearities, Chatter Generation and Suppression in Metal Cutting," Philos. Trans. R. Soc. London, Ser. A, **359**, pp. 663–693.

[2] Smith, S., and Tlusty, J., 1997, "Current Trends in High-Speed Machining," ASME J. Manuf. Sci. Eng., **119**, pp. 664–666.

[3] Tarng, Y., and Li, T., 1994, "The Change of Spindle Speed for the Avoidance of Chatter in End Milling," J. Mater. Process. Technol., **41**(2), pp. 227–236.

[4] Delio, T., Tlusty, J., and Smith, S., 1992, "Use of Audio Signals for Chatter Detection and Control," ASME J. Eng. Ind., **114**(2), pp. 146–157.

[5] Smith, S., and Tlusty, J., 1992, "Stabilizing Chatter by Automatic Spindle Speed Regulation," CIRP Ann., **41**(1), pp. 433–436.

[6] Choi, T., and Shin, Y., 2003, "On-Line Chatter Detection Using Wavelet-Based Parameter Estimation," ASME J. Manuf. Sci. Eng., **125**(1), pp. 21–28.

[7] Soliman, E., and Ismail, F., 1997, "Chatter Detection by Monitoring Spindle Drive Current," Int. J. Adv. Manuf. Technol., **13**(1), pp. 27–34.

[8] Faassen, R., Doppenberg, E., Wouw, N. v. d., Oosterling, J., and Nijmeijer, H., 2006, "Online Detection of the Onset and Occurrence of Machine Tool Chatter in the Milling Process," Second International Conference on High Performance Cutting, CIRP, Vancouver, Canada.

[9] Bickraj, K., Demutgul, M., Tansel, I., Kaya, B., and Ozcelik, B., 2008, "Detection of the Development of Chatter in End Milling Operations Using Index Based Reasoning (IBR)," ASME Early Career Technical Conference, ASME, Miami, FL.

[10] Eman, K. and S.M., W., 1980, "A Feasibility Study of On-Line Identification of Chatter in Turning Operations," ASME J. Eng. Ind., **102**, pp. 315–321.

[11] Insperger, T., Stépán, G., Bayly, P., and Mann, B., 2003, "Multiple Chatter Frequencies in Milling Processes," J. Sound Vib., **262**(2), pp. 333–345.

[12] Takemura, T., Kitamura, T., Hoshi, T., and Okushima, K., 1974, "Active Suppression of Chatter by Programmed Variation of Spindle Speed," CIRP Ann., **23**(1), pp. 121–122.

[13] Sastry, S., Kapoor, S. G., DeVor, R. E., and Dullerud, G. E., 2001, "Chatter Stability Analysis of the Variable Speed Face-Milling Process," ASME J. Manuf. Sci. Eng., **123**(4), pp. 753–756.

[14] Liu, K., and Rouch, K., 1991, "Optimal Passive Vibration Control of Cutting Process Stability in Milling," J. Mater. Process. Technol., **28**(1–2), pp. 285–294.

[15] Tarng, Y., Kao, J., and Lee, E., 2000, "Chatter Suppression in Turning Operations With a Tuned Vibration Absorber," J. Mater. Process. Technol., **105**(1–2), pp. 55–60.

[16] Zhang, Y., and Sims, N., 2005, "Milling Workpiece Chatter Avoidance Using Piezoelectric Active Damping: A Feasibility Study," Smart Mater. Struct., **14**(6), pp. N65–N70.

[17] Dohner, J., Lauffer, J., Hinnerichs, T., Shankar, N., Regelbrugge, M., Kwan, C., Xu, R., Winterbauer, B., and Bridger, K., 2004, "Mitigation of Chatter Instabilities in Milling by Active Structural Control," J. Sound Vib., **269**(1–2), pp. 197–211.

[18] Delio, T., 1992, "Method of Controlling Chatter in a Machine Tool," U.S. Patent No. 5,170,358.

[19] Soliman, E., and Ismail, F., 1998, "A Control System for Chatter Avoidance by Ramping the Spindle Speed," ASME J. Manuf. Sci. Eng., **120**, pp. 674–683.

[20] Eman, K., 1984, "Identification and Control of Chatter in Turning," Computer-Based Factory Automation, 11th Conference on Production Research and Technology, Pittsburgh, PA, pp. 413–417.

[21] Tlusty, J., and Polacek, M., 1963, "The Stability of Machine Tools Against Self-Excited Vibrations In Machining," ASME International Research in Production Engineering, Pittsburgh, PA, pp. 465–474.

[22] Ljung, L., 1999, *System Identification: Theory for the User*, 2nd ed., Prentice-Hall, Upper Saddle River, NJ.

[23] Haykin, S., 2002, *Adaptive Filter Theory*, 4th ed., Prentice-Hall, Upper Saddle River, NJ.

[24] Sayed, A., 2003, *Fundamentals of Adaptive Filtering*, Wiley-Interscience, New York.

[25] Faassen, R., Wouw, N. v. d., Oosterling, J., and Nijmeijer, H., 2003, "Prediction of Regenerative Chatter by Modelling and Analysis of High-Speed Milling," Int. J. Mach. Tools Manuf., **43**(14), pp. 1437–1446.

[26] Altintas, Y., 2000, *Manufacturing Automation*, Cambridge University Press, Cambridge, UK.

[27] Faassen, R., 2007, "Chatter Prediction and Control for High-Speed Milling: Modelling and Experiments," Ph.D. thesis, Eindhoven University of Technology, Eindhoven, The Netherlands.

[28] Duque, C., 2008, "Adaptive Gradient Lattice Prediction of a Multichannel IIR System in Adaptive Optics," MS thesis, TU Delft, Delft, The Netherlands.